Acta Cryst. (1979). A35, 431–445

X-ray and Neutron Diffraction from Liquid Alkali Metals

BY M. J. HUIJBEN AND W. VAN DER LUGT

Solid State Physics Laboratory, Materials Science Center, University of Groningen, Melkweg 1, *Groningen, The Netherlands*

(*Received* 28 *October* 1978; *accepted* 19 *December* 1978)

Abstract

This paper deals with the accurate determination of the structure factors of three liquid alkali metals: Na, K and Cs. Special attention has been paid to the experimental aspects: the design of the X-ray and neutron goniometers including the sample holders and the corrections to be applied to the rough experimental results. An assessment of the accuracy achieved has been made, mainly by comparison with existing physical data. In order to interpret the final results, theoretical calculations with hard-sphere models have been carried out and a comparison with the results of computer experiments, based on more realistic potentials, has been made. Some physical quantities related to the structure factor (pair distribution function, direct correlation function, pair potential and electrical resistivity) have been calculated.

I. Introduction

The purpose of the work described in this paper is the accurate determination of structure factors $S(q)$ of liquid metals. $S(q)$ is defined by

$$S(q)=\frac{1}{N}\sum_i\sum_j \exp\left[-i\mathbf{q}.(\mathbf{R}_i-\mathbf{R}_j)\right],$$

where N is the number of atoms considered and $\mathbf{R}_i$ are the positions of the atoms i. Accurate knowledge of structure factors is required for calculating other physical properties of these metals within the framework of the diffraction model (Ziman, 1961; Harrison, 1966). This work was stimulated by a paper by Greenfield, Wellendorf & Wiser (1971) and some of their ideas have been adopted, most particularly the use of transmission geometry.

This paper describes the construction of the equipment for X-ray and neutron diffraction and outlines the rather laborious correction procedures to be applied to the experimental results. Subsequently, results for pure Na, K and Cs are presented and the accuracy that has been achieved is discussed. Finally, the results are interpreted with the help of existing theories of the liquid structure and some related properties are discussed.

This investigation is described in more detail in the thesis of the first author, a few copies of which are available for distribution. It was followed by an investigation of the liquid Na/Cs binary system, which will be communicated elsewhere.

II. The experimental arrangement

(*a*) *The apparatus for X-ray diffraction*

Adopting the arguments of Greenfield, Wellendorf & Wiser (1971) we used a transmission geometry for our experiments. To carry out diffraction experiments on highly reactive alloys, a liquid-metal sample holder was designed, which fulfils a number of special conditions (Fig. 1).

It is necessary to vary the thickness of the samples. Because of the large difference in mass absorption

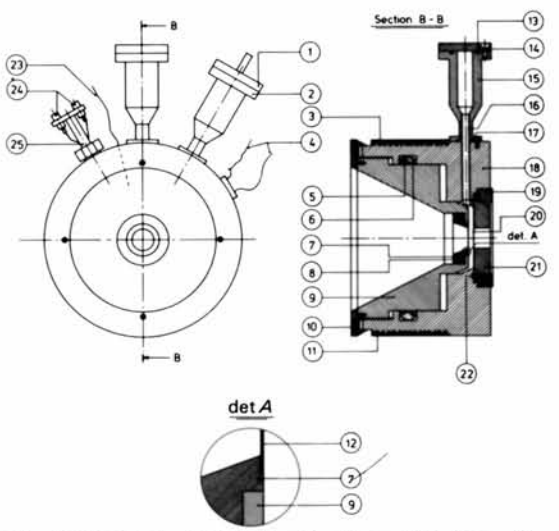

Fig. 1. Liquid-metal sample holder for X-ray diffraction using the transmission method. Numbers indicated in the figure are explained in the text.

0567-7394/79/030431-15$01.00

coefficient between the alkali metals, the optimum layer thickness of the sample varies from one sample to another. The vacuum tightness of the sample holder has to be sufficient to prevent air from entering. The windows of the sample holder are chosen such that the transmission of the radiation through the windows is as high as possible and the diffraction pattern of the windows consists of only a few narrow Bragg peaks.

It is not easy to fulfil all these conditions in one and the same goniometer. The requirement that sometimes very thin (down to 0·1 mm) samples are needed especially offers some mechanical problems. This problem is solved by soldering a thin Be sheet [0·2 mm thick and 18·0 mm in diameter, (12)] to a kovar holder (7) as depicted in the inset in Fig. 1. This Be holder can be screwed into a bigger part (9) of the sample holder. The other Be window [0·1 mm thick and 55·0 mm in diameter, (20)] is pressed by (19) and (21) against the back of the sample holder (18). The sample holder itself, made of brass, is plated with Ni to avoid corrosion by the alkali metals. By screwing the two parts into each other, it is possible to vary the distance between the two windows continuously. The adjustable distance allows a spacing of 4 mm between the two windows and, afterwards, the reduction of the sample thickness appropriately. The sample holder can be filled *via* two tubes [(2) and (15)] on top of it. A set of viton rings [(5), (8), (13), (17) and (22)] prevents air from entering the sample holder during adjustment of the spacing between the windows as well as during the actual diffraction experiment. A heating wire (11) is wound round the sample holder and can be connected to a temperature-controlling unit. An NTC resistor is screwed into the holder by (25) to measure the temperature; after calibration of the resistor, the temperature can be adjusted within ±0·5 K with this controlling unit. Additionally, to determine accurately the temperature of the sample, a copper–constantan thermocouple (23) is mounted in a narrow cylindrical hole, close to the sample.

An existing, hand-rotated horizontal goniometer (Société des Instruments Physique Genèvoise PD-2) was adapted to the requirements of this experiment. The optical system used for the X-ray transmission measurements is illustrated in Fig. 2. The X-ray beam

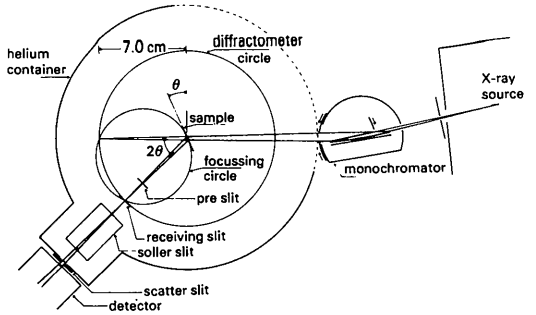

Fig. 2. The optical system for the X-ray transmission measurements.

from a Mo line source monochromatized with a curved quartz crystal (de Wolff, 1948) is limited by a diaphragm in the monochromator housing and a slit system at the end of the monochromator housing. The quartz crystal is bent so as to conform to a logarithmic spiral, with the origin at the focal spot. For maintaining exact focusing at all scattering angles, the sample has to be rotated about its own axis, with an angular velocity half that of the detector. The advantage of this type of monochromator is that it gives a large distance between the monochromator and the focal spot. This is required by the large dimensions of our sample holder.

The scattered beam is collimated by a system of two slits, of which the pre-slit is large enough to accept all radiation scattered from the sample at any angle 2θ for which measurements are performed. The divergence of this pre-slit is 2°. A 0·2 mm receiving slit is used. Horizontal Soller-slits prevent spurious scattering from entering the detector. A scatter slit with an opening of approximately 2 mm is placed just in front of the detector.

To minimize air scattering, the equipment (apart from the detector and monochromator) is placed in a container in which a He atmosphere is maintained. Mylar windows with a thickness of 6 μm allow the X-ray beam to penetrate the container without appreciable absorption.

For detection, a scintillation counter and a pulse-height discriminator are used. The spectrum is determined by the 'fixed number of counts' method, which reduces the intensity measurement to a time measurement. Data are taken at intervals of $\frac{1}{4}°$ covering a range of $2\theta = 1·75$ to 55°.

(*b*) *The apparatus for neutron diffraction*

For this experiment a quite different sample holder was designed (Fig. 3).

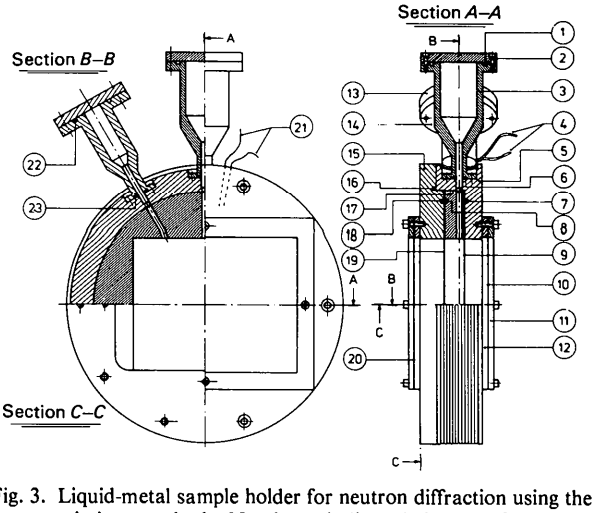

Fig. 3. Liquid-metal sample holder for neutron diffraction using the transmission method. Numbers indicated in the figure are explained in the text.

A neutron beam with a cross section 25 × 25 mm is used. For technical convenience a fixed sample thickness of 10·0 mm is chosen. This is provided for by clamping a spacer (17) of 10·0 mm thickness between two brass blocks [(5) and (15)]. To avoid corrosion, the sample holder is plated with Ni. A set of viton rings [(1), (6), (7), (8), (16) and (17)] prevents air from entering the sample holder. The windows [(9) and (19)] are made of V sheets, because V is an incoherent scatterer and produces only a constant background intensity. A heating wire (4) can be wound round the sample holder; a temperature-control system provides a constant (±0·5 K) temperature. To reduce the temperature gradient along the sample, two Al foils [(10) and (20)], each stretched in a framework [(11) and (12)], are screwed against the outside of the sample holder. Then the air enclosed between the V sheets and the Al foils is heated to approximately the same temperature as the sample holder. In this way, a smaller temperature gradient over the sample is obtained. Two thermocouples (21), one for automatic adjustment of the temperature and the other for measuring the temperature, are mounted each in a cylindrical hole close to the sample.

The neutron beam is provided by the static reactor of the ECN (Energy Centre Netherlands), Petten. The optical system for the neutron measurements is shown in Fig. 4. To monochromatize the neutron radiation, use is made of highly oriented pyrolytic graphite which has a high reflectivity and a satisfactory momentum and energy resolution. The monochromator is cylindrically bent (R = 600 mm); the axis of the cylinder is in the plane of diffraction defined by the incoming and outgoing wavevectors. The purpose of this bending of the monochromator is to increase the neutron flux at the position of the sample (Riste, 1970; Nunes & Shirane, 1971).

A second block of pyrolytic graphite (diameter 50 mm, length 60 mm) removes the half-wavelength contamination of the 12·3 meV radiation transmitted by the monochromator. This is accomplished with only a small reduction in the number of neutrons of the desired wavelength.

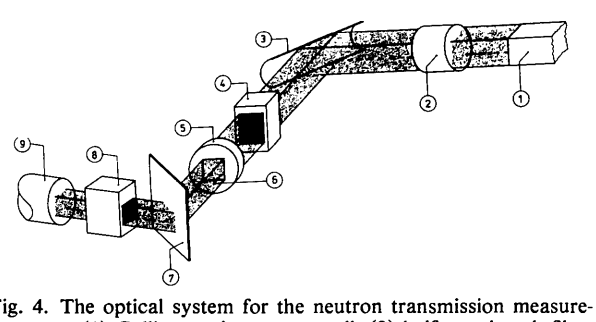

Fig. 4. The optical system for the neutron transmission measurements. (1) Collimator in reactor wall, (2) half-wavelength filter, (3) monochromator, (4) Soller slits, (5) small-absorption detector, (6) opening to limit the beam, (7) sample, (8) Soller slits, (9) detector.

In this experiment, neutrons of two different energies (12·3 and 44·2 meV corresponding to 2·58 and 1·36 Å) are used to increase the accuracy of the results in the entire range of scattering wavevectors from q = 0·1 to 6·5 Å^{-1}.

After monochromatization of the collimated beam, two vertical Soller slits are used to limit the horizontal divergence of the beam. These Soller slits consist of Cd-coated Ni plates. The angular aperture of any pair of adjacent plates is 30 and 40′ for the first and second set of Soller slits, respectively.

The beam has to pass through a 25 × 25 mm opening in a Cd plate situated between the first set of Soller slits and the sample. For detection of the scattered radiation a BF_3 gas counter is used.

An automatically driven goniometer with a step-scan facility was put at our disposal by the ECN. Each step is initiated by an electrical pulse. The time interval between the pulses depends on the neutron flux: each interval corresponds to an equal, preset number of incoming neutrons. In order to achieve this, the incoming neutrons are counted by a second detector, which absorbs only a small fraction of the neutron flux. When the appropriate number of neutrons has passed, a pulse is given to an on-line computer, which takes care of the correct rotation of the detector and the sample. The angle of rotation of the sample is just half the angle of rotation of the detector. The angles of rotation are such that each step corresponds to 0·04 Å^{-1} when λ = 2·58 Å and to 0·1 Å^{-1} when λ = 1·36 Å.

(c) *The metals*

Pure K and Cs were commercially obtained from Kawecki with a nominal purity of 99·9998% and 99·98%, respectively. Na metal was obtained from Merck with a nominal purity of 99·93%.

III. Analysis of the experimental results

(a) *Analysis of the X-ray diffraction measurements*

The experimentally determined X-ray intensities have to be subjected to several corrections before they can be converted into structure factors. Corrections are required for absorption, polarization, Compton scattering (also referred to as incoherent or inelastic scattering) and multiple scattering. Additionally, a normalization procedure has to be applied. Since the mathematical procedures are quite laborious, computer programs were organized to carry out these corrections.

Smelser, Henninger, Pings & Wignall (1975) have investigated the efficiency of several *monochromatizing techniques*. From their work it follows that the effect of the angle dependence of the radiation intensity, caused by the monochromatizing procedure,

is negligible in studies of liquid structure with a curved crystal monochromator.

Because the X-rays are scattered not only by the sample but also by the container and other auxiliary parts, we have to correct for *empty-cell scattering*. Therefore we have to carry out two different experiments, one with an empty sample holder [intensity $I_c(2\theta)$] and one with the sample holder filled with the liquid metal [intensity $I_{cs}(2\theta)$]. As a matter of course, $I_c(2\theta)$ forms part of $I_{cs}(2\theta)$ but it is modified by the *absorption* of the liquid sample. An important quantity entering the calculation of the absorption and scattering corrections is the *path length* of the radiation within the sample. If t_s is the thickness of the sample, this length is $t_s/\cos\theta$ where θ is the angle of incidence. As a consequence, both absorption and scattering corrections depend on θ.

When X-rays are used, *polarization of the radiation* is caused by the monochromator crystal and by the sample. The expression for the polarization factor is discussed by Kerr & Ashmore (1974) for different monochromator crystals and two common designs for the diffractometer. In our case, we have to apply the following expression [equation (3) of Kerr & Ashmore (1974)]:

$$P(2\theta) = \frac{1 + |\cos 2\theta_m| \cos^2 2\theta}{1 + |\cos 2\theta_m|}, \qquad (3.1)$$

where $2\theta_m$ is the Bragg angle of the monochromator crystal. The intensity scattered by the sample only, expressed in arbitrary units, is given by

$$I_s(2\theta) = [P(2\theta) A_{sc}(2\theta)]^{-1} \times [I_{cs}(2\theta) - A_s(2\theta) I_c(2\theta)], \qquad (3.2)$$

where $A_{sc}(\theta)$ and $A_s(2\theta)$ are the correction factors for radiation absorbed by the sample + cell-windows and scattered by the sample, and for radiation absorbed by the sample only, respectively:

$$A_{sc}(2\theta) = \frac{t_s}{\cos\theta} \exp\left[-(\mu_c t_c + \mu_s t_s)/\cos\theta\right], \qquad (3.3)$$

$$A_s(2\theta) = \exp\left(-\mu_s t_s/\cos\theta\right). \qquad (3.4)$$

The quantities t_c, t_s and μ_c, μ_s are the thicknesses and linear absorption coefficients, respectively.

The products $\mu_c t_c$ and $\mu_s t_s$ can be readily obtained from experiments by measuring the intensity of the beam before and after introducing the cell-windows and the liquid sample into the cell, respectively. We had to reduce the voltage of the generator to such a low value that the $\lambda/2$ wavelength was not excited, because the brass absorber, which was introduced for attenuating the central beam, leads to preferential hardening of the radiation and consequently to an incorrect determination of the linear absorption coefficient.

To determine the structure factor from the experimental X-ray data for a pure liquid metal, the measured intensity has to be reduced to an intensity per atom. Therefore, a *normalization procedure* is introduced; it provides a normalization factor β:

$$I_a^{\text{tot}}(q) = \beta I_s(q), \qquad (3.5)$$

where $q = 4\pi \sin\theta/\lambda$. Any q dependence of β, due to the geometrical configuration of the experiment, proves to be negligible.

In our experimental arrangement the intensity $I_a^{\text{tot}}(q)$ contains the intensity due to elastic scattering $I_a^{\text{el}}(q)$, which is the quantity we are interested in, the intensity due to inelastic scattering $I_a^{\text{inel}}(q)$ and the intensity due to multiple scattering $I_a^{\text{ms}}(q)$. Therefore

$$I_a(q) = I_a^{\text{el}}(q) = I_a^{\text{tot}}(q) - I_a^{\text{inel}}(q) - I_a^{\text{ms}}(q). \qquad (3.6)$$

The inelastic and multiple scattering terms must be eliminated and this is accomplished by calculating them in an appropriate approximation. The structure factor $S(q)$ of the liquid is then given by:

$$S(q) = [\beta I_s(q) - I_a^{\text{inel}}(q) - I_a^{\text{ms}}(q)]/f^2(q). \qquad (3.7)$$

The *atomic scattering factors* $f(q)$ are adopted from calculations by Doyle & Turner (1968). To account for anomalous dispersion one must introduce a complex scattering factor. The real and imaginary dispersion corrections are expected to be independent of the scattering angle for Na, K and Cs and values for these corrections are presented by Cromer & Liberman (1970).

The best procedure to correct for the *inelastic (Compton) scattering* is to calculate it rather than to eliminate it experimentally. Theoretical values have been computed by Cromer & Mann (1967). These inelastic scattering factors do not include the Breit–Dirac recoil factor. Therefore the tabulated data must be multiplied by the factor $R = (\lambda'/\lambda)^2$ when counters and scalers are used as detectors.

The intensity due to inelastic scattering, however, is attenuated by a different absorption factor (Hajdu & Palinkas, 1972), because the wavelength of the Compton radiation changes under scattering which gives a slightly different linear absorption coefficient after scattering. If the linear absorption coefficient is written as

$$\mu(\lambda) = \mu_s + \Delta\mu(\lambda), \qquad (3.8)$$

where μ_s is the linear absorption coefficient at the wavelength of the incident radiation, one can calculate the absorption factor for the intensity due to inelastic scattering to be:

$$A'_{sc}(2\theta) = \exp\left[-(\mu_c t_c + \mu_s t_s)/\cos\theta\right] \times [1 - \exp\left(-\Delta\mu t_s/\cos\theta\right)]/\Delta\mu. \qquad (3.9)$$

Evaluating the correction for the inelastically-scattered radiation, we first multiply the intensity of the Compton radiation by the factor

$$\frac{\cos\theta}{t_s\,\Delta\mu}\,[1-\exp(-\Delta\mu t_s/\cos\theta)] \qquad (3.10)$$

and next we apply the absorption correction as given in (3.3). Using Victoreen's formula (*International Tables for X-ray Crystallography*, 1962), we can write for $\Delta\mu$:

$$\Delta\mu=\rho\frac{h}{mc}\,2\sin^2\theta(3C\lambda^2-4D\lambda^3). \qquad (3.11)$$

C and D are constant for a given element and wavelength (*International Tables for X-ray Crystallography*, 1962).

The mathematical description for the *double scattering correction* is given by Malet, Cabos, Escande & Delord (1973). To calculate this correction the structure factor is needed, so an iterative procedure is followed starting with a structure factor which is taken as unity at all scattering angles.

To obtain the intensity due to *multiple scattering*, one assumes that the ratio between the $(n+1)$th order scattering and the nth order scattering is of the same order as the ratio between the second and the first order scattering. Then $I_a^{ms}(q)$ can be found by summing a geometrical series:

$$I_a^{ms}(q)=I_a^{(2)}(q)+I_a^{(3)}(q)+I_a^{(4)}+\ldots$$
$$=\frac{I_a^{(2)}(q)}{[1-I_a^{(2)}(q)/I_a^{(1)}(q)]}. \qquad (3.12)$$

The normalization factor β is obtained by Fourier transforming $S(q)-1$ and making use of the fact that the radial distribution function $g(r)$ is zero when r approaches zero:

$$\int_0^\infty [S(q)-1]\,q^2\,dq=-2\pi^2\rho_0. \qquad (3.13)$$

We can find the normalization constant β by substituting the structure factor (3.7) into (3.13):

$$\beta=\frac{\int_0^{q_{max}} q^2\{[I_a^{inel}(q)+I_a^{ms}(q)]/f^2(q)+1\}\,dq-2\pi^2\rho_0}{\int_0^{q_{max}} q^2[I_s(q)/f^2(q)]\,dq}. \qquad (3.14)$$

The upper limit of integration has been replaced by the value q_{max} chosen such that, with sufficient accuracy, $S(q)=1$ for $q>q_{max}$ [or $I_a^{el}(q)=f^2(q)$ for $q>q_{max}$].

(*b*) *Analysis of the neutron diffraction measurements*

As for the X-ray results, the neutron diffraction results require several corrections before an accurate structure factor can be determined. In this case, the experimental results must be corrected for absorption, incoherent scattering, inelastic scattering and multiple scattering; also, a different normalization procedure is needed.

To start with, the total scattered intensity must be corrected for *background radiation*. The background scattering originates from cell scattering and from spurious fast neutrons. The contribution from the fast neutrons is measured with the 25 × 25 mm opening covered by Cd plates. With the *absorption corrections* applied we come to the following formula:

$$I_s(2\theta)=[A_{sc}(2\theta)]^{-1}\{I_{cs}(2\theta)-A_s(2\theta)\,[I_c(2\theta)-I_c^{fast}(2\theta)]-I_{cs}^{fast}(2\theta)\}, \qquad (3.15)$$

where I_{cs}, I_{cs}^{fast} and I_c, I_c^{fast} are the total intensity and the fast neutron intensity scattered by sample + cell and cell only, respectively. $A_{sc}(2\theta)$ and $A_s(2\theta)$ are correction factors, $A_{sc}(2\theta)$ for the neutrons absorbed by the sample + cell-windows and scattered by the sample, and $A_s(2\theta)$ for the neutrons absorbed by the sample only:

$$A_{sc}(2\theta)=\frac{t_s}{\cos\theta}\exp[-(\tau_c+\tau_s)/\cos\theta] \qquad (3.16)$$

and

$$A_s(2\theta)=\exp[-\tau_s/\cos\theta]. \qquad (3.17)$$

In the present case $\tau_s=\sigma_{T,s}t_s\rho_s$ where $\sigma_{T,s}$ is the total cross section of the sample, t_s is the thickness of the sample and ρ_s is the number of atoms per unit volume of the sample. $\tau_c=\sigma_{T,c}t_c\rho_c$ is defined analogously for the windows. The total cross section contains contributions from coherent scattering, incoherent scattering and true absorption:

$$\sigma_T=\sigma_{coh}+\sigma_{inc}+\sigma_{abs}. \qquad (3.18)$$

The values quoted by Shull (1971) are listed in Table 1 for Na and Cs. From our measurements it follows that the quoted value for σ_{inc} (Cs) is wrong (see § V).

The structure factor of a liquid sample can be calculated from the neutron experiments by the following procedure. The corrected scattered intensity is multiplied by a normalization factor β and the

Table 1. *The cross sections for* Na *and* Cs *at the wavelengths used*

For σ_{inc} (Cs), see also § V.

σ (*b*)	Na	Cs
σ_{coh}	1·55	3·8
σ_{inc}	1·85	3·2
σ_{abs} (1·36 Å)	0·404	25·1
σ_{abs} (2·58 Å)	0·766	44·1

intensities due to incoherent, inelastic and multiple scattering are subtracted. This gives for $S(q)$:

$$S(q) = \left\{ \beta I_s(q) - \frac{\sigma_{inc}}{4\pi}[1 + P(q)_{inc}] - I_a^{ms}(q) - \frac{\sigma_{coh}}{4\pi} P(q)_{coh} \right\} \Big/ \frac{\sigma_{coh}}{4\pi}. \quad (3.19)$$

The *inelastic scattering* $P(q)$ arises from collision processes in which energy is transferred from the neutron to a nucleus or *vice versa*. These processes can be described in terms of the dynamic structure factor $S(q,\omega)$ (*e.g.* Marshall & Lovesey, 1971). The inelastic scattering is often referred to as a Placzek correction.

Many authors have given attention to the calculation of the contribution from inelastic scattering. We mention Placzek (1952), Powles (1973*a*,*b*), Rahman, Singwi & Sjölander (1962*a*,*b*), Ascarelli & Gagliotti (1966) and Yarnell, Katz, Wenzel & Koenig (1973). The last method differs from those of the other authors in that the energy dependence of the efficiency of the radiation detector is introduced more explicitly. This result can be adapted most easily to our work. We have taken into account the Placzek corrections for coherent as well as for incoherent scattering. The expression used for the correction of the inelastic scattering can be written as equation (A14) in the paper by Yarnell, Katz, Wenzel & Koenig (1973):

$$P(q) = -\frac{m}{M}\left[\frac{k_B T}{2E_0} - \left(C_1 + C_3 \frac{k_B T}{E_0} - \frac{m}{2M}\right)\right], \quad (3.20)$$

where m is the mass of the neutron, M the mass of the atom and E_0 the energy of the incident neutron. The constants C_1 and C_3 are related to the energy dependence of the detector. In our case: $C_1 = 0{\cdot}836$, $C_3 = 0{\cdot}240$ for $\lambda = 1{\cdot}36$ Å; $C_1 = 0{\cdot}952$, $C_3 = 0{\cdot}113$ for $\lambda = 2{\cdot}58$ Å.

For calculating the *double scattering* of thermal neutrons, the formulation of Vineyard (1954) (see also Cocking & Heard, 1965) was adopted for a plane sample geometry in the approximation of an isotropic cross-section. The intensity due to *multiple scattering* is calculated in the same way from the double scattering as was done for X-rays. Because the neutron experiments are carried out for two different neutron wavelengths, the *normalization procedure* includes matching of the two kinds of experiments. The normalization constant β is determined from the experiments at $\lambda = 1{\cdot}36$ Å. From (3.19) for the neutron interference function one finds

$$\beta = \left\{ \int_{q_{min}}^{q_{max}} \left\{ \frac{\sigma_{coh}}{4\pi}[1 + P(q)_{coh}] + \frac{\sigma_{inc}}{4\pi}[1 + P(q)_{inc}] + I_a^{ms}(q) \right\} dq \right\} \left[\int_{q_{min}}^{q_{max}} I_s(q)\, dq \right]^{-1}, \quad (3.21)$$

where q_{min} is the minimum value of q beyond which the structure factor is essentially constant [or $I_a^{el}(q)$ is equal to $\sigma_{coh}/4\pi$], and q_{max} is the maximum q value covered by the experimental data. With this normalization factor, the neutron interference function is defined for the small-wavelength neutron experiment. The normalization factor for the long-wavelength neutron experiment can be calculated by comparing the two measurements in the region of overlap.

IV. Discussion of the X-ray measurements

(*a*) *Results*

We have performed X-ray experiments on liquid Na, K and Cs. Experiments on liquid Rb were not feasible with our geometry because of the relatively large fluorescence scattering of this element. Similar experiments on Na and K have been performed by Greenfield, Wellendorf & Wiser (1971). We repeated them to estimate the discrepancies between the two measurements, which both aimed for high accuracy. As far as the authors know, the measurements on liquid Cs were the first obtained in this way (see also Huijben & van der Lugt, 1976). Figs. 5, 6 and 7 show the structure factors for Na, K and Cs, each at several temperatures, from the melting point onward. For $q < 0{\cdot}31$ Å^{-1} the structure factors were found by extrapolation. With rising temperature, the height of the first peak decreases gradually, whereas its width increases correspondingly.

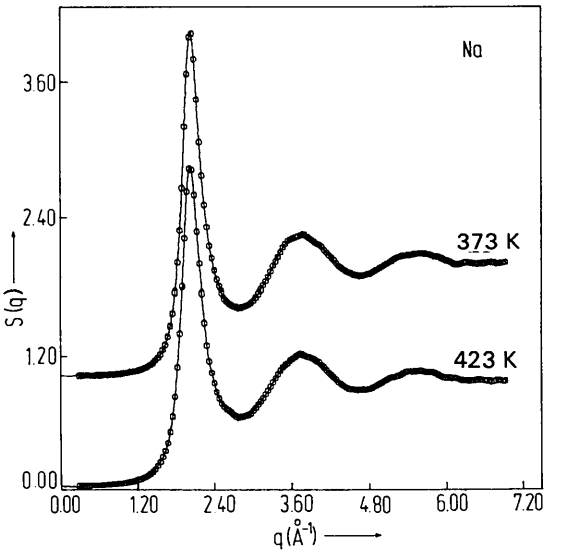

Fig. 5. The experimental structure factors of liquid Na at different temperatures.

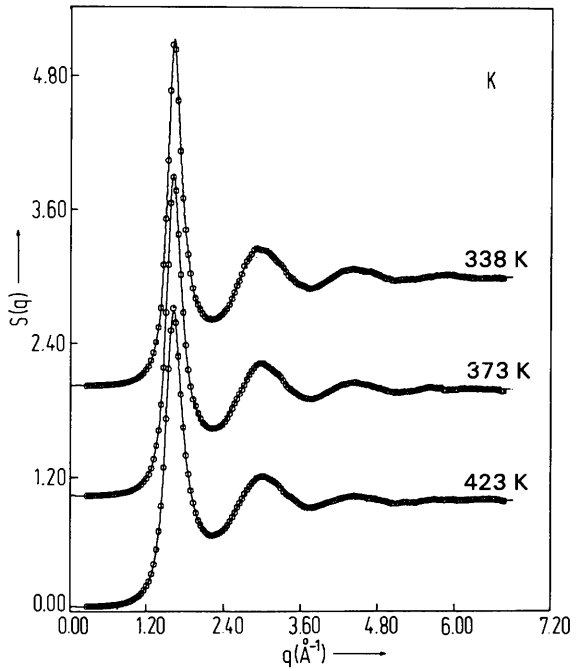

Fig. 6. The experimental structure factors of liquid K at different temperatures.

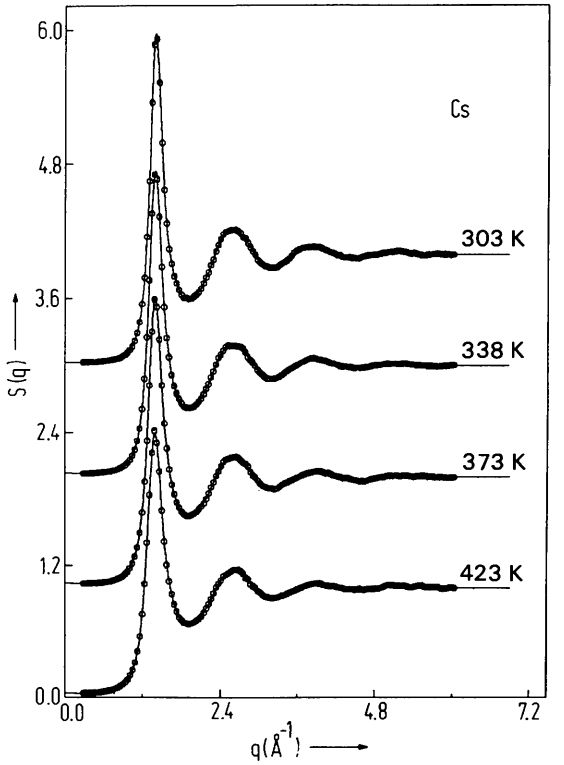

Fig. 7. The experimental structure factors of liquid Cs at different temperatures.

More generally, the oscillations in $S(q)$ become progressively damped at high temperatures. This is a consequence of the blurring of the liquid structure. In Figs. 8, 9 and 10, this effect is demonstrated more specifically for the low-q region. On the other hand, the position of the first peak proves to be independent of temperature.

Denoting by q_1 the position of the first peak and by S^{mp} the structure factor close to the melting point T_{mp} we have plotted $S(q_1)/S^{mp}(q_1)$ as a function of the reduced temperature T/T_{mp} (Fig. 11). The data for all three metals, Na, K and Cs, are represented by a single straight line. Wagner (1977) observed the same behaviour for Sn, Ga, Zn and Cd, although the straight line shared by these metals is different from the one found for the alkali metals.

Fig. 12 illustrates an attempt to match the structure factors for Na, K and Cs as precisely as possible by scaling the q values. All data pertain to the melting points. Evidently, this attempt is fairly successful even for small angles. We find a constant ratio (1·83) between q_2 [the position of the second maximum in $S(q)$] and q_1 for Na, K and Cs. This is in agreement with the findings of Waseda & Suzuki (1973).

(*b*) *Comparison of* $S(0)$ *with compressibility data*

Between $S(0)$, as found by extrapolation, and the isothermal compressibility χ_T, the following relation exists:

$$S(0) = \rho_0 k_B T \chi_T, \qquad (4.1)$$

where ρ_0 is the number density of atoms.

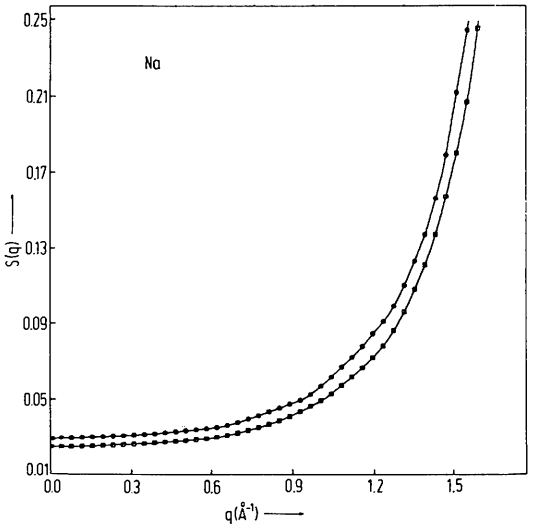

Fig. 8. Small-angle range of the structure factors of liquid Na at different temperatures. For $q < 0{\cdot}31$ Å^{-1}, the measured structure factors were obtained by extrapolation. For this purpose, the experimental data were suitably smoothed. □ $T = 373$ K, ○ $T = 423$ K.

As χ_T is experimentally not easily accessible, we have used the adiabatic values, χ_s, found from sound velocity measurements, and corrected them according to

$$\chi_T = \left(1 + \frac{TV_m \alpha_p^2}{\chi_s C_p}\right) \chi_s, \tag{4.2}$$

$$\chi_s^{-1} = \rho v_s^2. \tag{4.3}$$

Here, v_s is the sound velocity, ρ the density, V_m the molar volume, C_p the heat capacity at constant pressure and α_p the thermal expansion coefficient.

From density measurements (Huijben, Klaucke, Hennephof & van der Lugt, 1975; Huijben, van Hasselt, van der Weg & van der Lugt, 1976) we know ρ, V_m and α_p. Sound velocity data were obtained from Kim, Kemp & Letcher (1971), who also reported values for the heat capacity.

In Table 2 the experimental $S(0)$ are compared with calculated values of $\rho_0 k_B T \chi_T$. The $S(0)$ values are 5 to 20% higher than those calculated from the sound velocity data. Also, the values of the sound velocity found in the literature show serious discrepancies among themselves (Novikov, Trelin & Tsyganova, 1970; Chan, 1972; Faber, 1972); those by Kim, Kemp & Letcher (1971) were considered the best. Furthermore, the extrapolation of the structure factor to $q = 0$ is subject to some arbitrariness. An error of 5 to 10% is easily introduced.

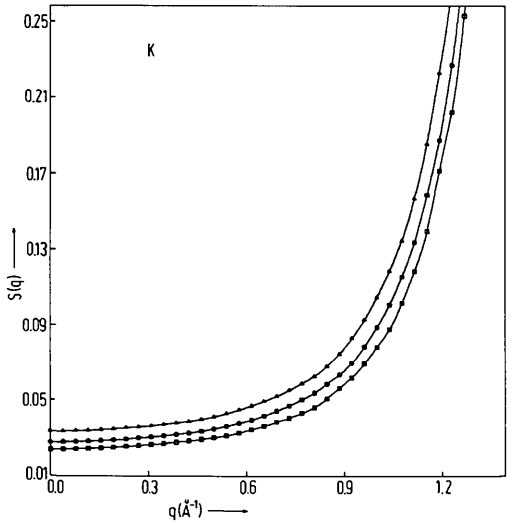

Fig. 9. As Fig. 8, for K. □ $T = 338$ K, ○ $T = 373$ K, △ $T = 423$ K.

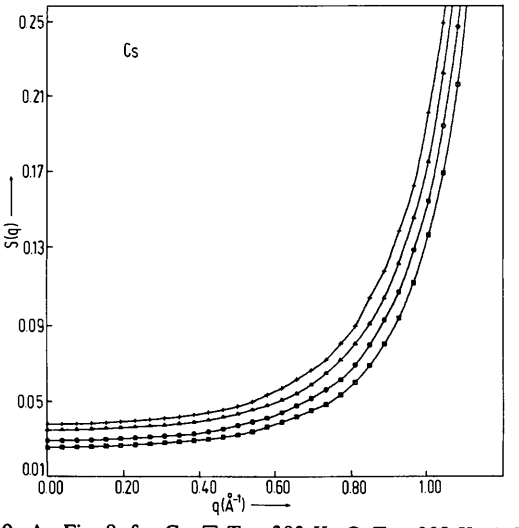

Fig. 10. As Fig. 8, for Cs. □ $T = 303$ K, ○ $T = 338$ K, △ $T = 373$ K, + $T = 423$ K.

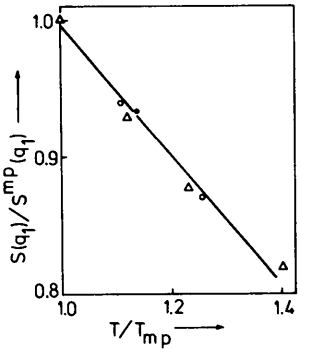

Fig. 11. Ratio of the height $S(q_1)$ of the first peak at different temperatures to that observed close to the melting point as a function of the reduced temperature T/T_{mp}. The data are represented by ● for liquid Na, ○ for liquid K and △ for liquid Cs.

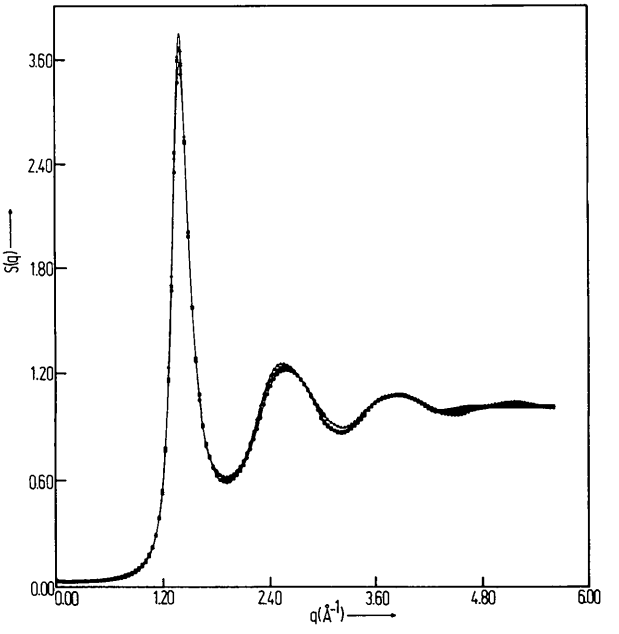

Fig. 12. The structure factors $S(q)$ of Na, K and Cs just above their melting points after scaling the q values. The scale of the abscissa corresponds to Cs. □ Na, 373 K; △ K, 338 K; ○ Cs, 303 K.

Table 2. χ_T, $S(0)$ *and* $\rho_0 k_B T\chi_T$ *for* Na, K *and* Cs *at a few temperatures, the sixth column gives the deviation of* $S(0)$ *from* $\rho_0 k_B T\chi_T$

Additionally, some values of $\rho_0 k_B T\chi_T$ (Faber, 1972) are listed.

	T (K)	χ_T (m s^2 g^{-1}) × 10^8	$S(0)$	$\rho_0 k_B T\chi_T$	$\frac{S(0)-\rho_0 k_B T\chi_T}{S(0)}$ (%)	$\rho_0 k_B T\chi_T$ (Faber)
Na	373	0·194	0·0256	0·0242	5	0·024
	423	0·205	0·0302	0·0286	5	
K	338	0·384	0·0241	0·0228	5	0·023
	373	0·401	0·0279	0·0260	7	
	423	0·426	0·0335	0·0309	8	
Cs	303	0·620	0·0256	0·0215	16	0·028
	338	0·649	0·0292	0·0249	15	
	373	0·679	0·0348	0·0284	18	
	423	0·725	0·0379	0·0339	11	

(c) *Comparison with results obtained by other authors*

When comparing our data for Na and K with those of Greenfield, Wellendorf & Wiser (1971) (GWW), we should be aware of the difference between the respective experimental equipments. GWW worked with a symmetrically-bent monochromator crystal and detected a divergent beam, whereas we worked with an asymmetrically-bent monochromator crystal enabling the detection of a focused beam, which results in better resolution.

Also, the correction procedures used by GWW are slightly different. The most important difference originates from our inclusion of the multiple-scattering correction. For the structure factor at $q = 0$ this term appears to give a contribution of 17%, 18% and 32%, for Na, K and Cs, respectively, at their respective melting temperatures. The influence of the multiple scattering correction for larger q values is rather small, especially for Cs, and, for q values beyond the first peak, it never exceeds 2% of the total intensity.

Nevertheless, the structure factors obtained by GWW and those obtained in our experiments compare favourably (Fig. 13) as the deviations never exceed 10% for Na and 16% for K (Fig. 14), the largest differences occurring for values of q up to and including the first peak in the structure factor. For small q the discrepancies can be attributed to the different treat-

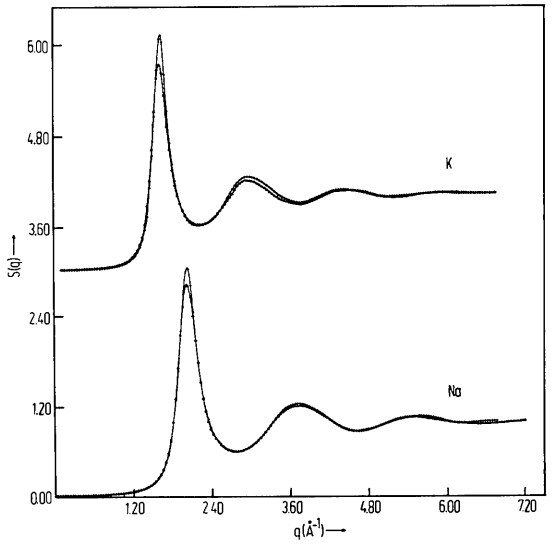

Fig. 13. $S(q)$: comparison of our data (+: upper curves) for Na at 373 K and K at 338 K with those obtained by Greenfield, Wellendorf & Wiser (1971) (△: lower curves).

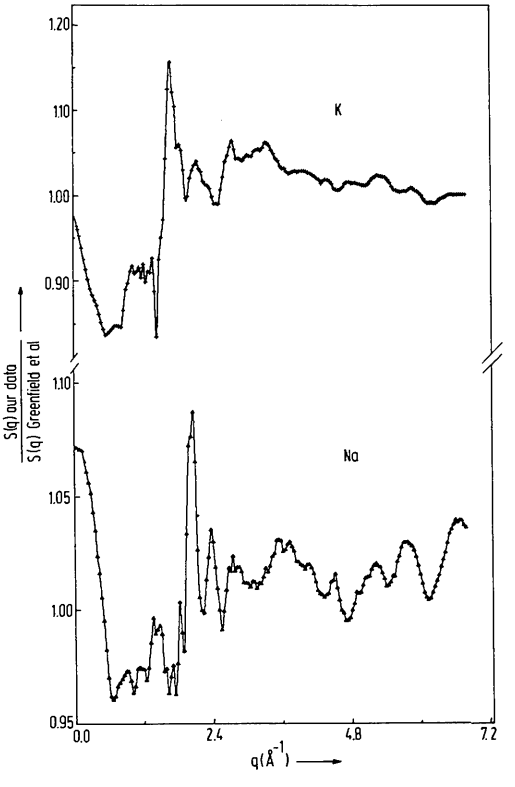

Fig. 14. The ratio of the experimental values of $S(q)$ as determined by ourselves and by Greenfield, Wellendorf & Wiser (1971). The data pertain to Na at 373 K and K at 338 K.

ment of the multiple scattering, whereas at the first peak the difference in resolution of the two detection systems may be the main cause of the discrepancies.

GWW, in Fig. 4 of their paper, compare their results for Na at 373 K with those obtained previously by different authors. We may refer to this paper for such a comparison and only remark here that the discrepancies between GWW's and our results are much smaller than those between GWW's or our results on the one hand and the earlier results on the other.

Schierbrock, Langner, Fritsch & Lüscher (1972) and Kollmansberger, Fritsch & Lüscher (1970) have employed an X-ray reflection technique to obtain $S(q)$ for Na at 387·3 and 375·1 K, respectively. In both geometries the monochromator crystal is placed in the reflected beam. For $q < 1{\cdot}0$ Å^{-1}, they obtain slightly larger values than we do. For a more detailed comparison, the reader is referred to the respective papers.

In Fig. 15 the present results for the structure factor of liquid Cs are compared with the neutron diffraction results by Gingrich & Heaton (1961). A remarkable phase shift is observed. Also, the normalization procedure used by Gingrich & Heaton seems to be not entirely correct.

The graphs representing the neutron diffraction results obtained by Oehme & Richter (1966) for Na and Cs are unsuitable for quantitative comparison.

(*d*) *Radial distribution functions and direct correlation functions*

In the theory of liquids, the radial distribution function $g(r)$ and the direct correlation function $c(r)$ play an important role. The radial distribution function is obtained from the Fourier transform of $S(q) - 1$ by

$$g(r) = 1 + \frac{1}{2\pi^2 \rho_0 r} \int_0^\infty [S(q) - 1]\, q \sin qr \, dq. \quad (4.4)$$

The errors which may arise in calculating $g(r)$ from the measured $S(q)$ are discussed by Paalman & Pings (1963) and by Wagner (1972). The direct correlation function $c(r)$ is defined by the Ornstein–Zernike relation

$$g(r) - 1 = c(r) + \rho_0 \int c(|\mathbf{r} - \mathbf{r}'|)\, \{g(r') - 1\}\, d\mathbf{r}'. \quad (4.5)$$

It can be calculated from $S(q)$ by

$$c(r) = \frac{1}{2\pi^2 \rho_0 r} \int_0^\infty \frac{[S(q) - 1]}{S(q)}\, q \sin qr \, dq. \quad (4.6)$$

Figs. 16, 17 and 18 illustrate the results for $g(r)$ for Na, K and Cs, respectively. The deviations from zero at small r as well as the irregularity in the right-hand side slope of the first peak result from the truncation, at a large value of q, of the experimental structure factors.

From $g(r)$ the number of nearest neighbors (coordination number) can be calculated from

$$N = 4\pi\rho_0 \int_{r_1}^{r_2} r^2 g(r)\, dr, \quad (4.7)$$

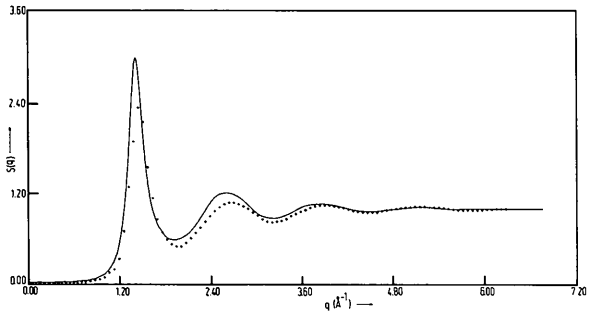

Fig. 15. The present X-ray diffraction results (——) compared with the neutron diffraction results of Gingrich & Heaton (1961) (+ + +) for liquid Cs at 303 K.

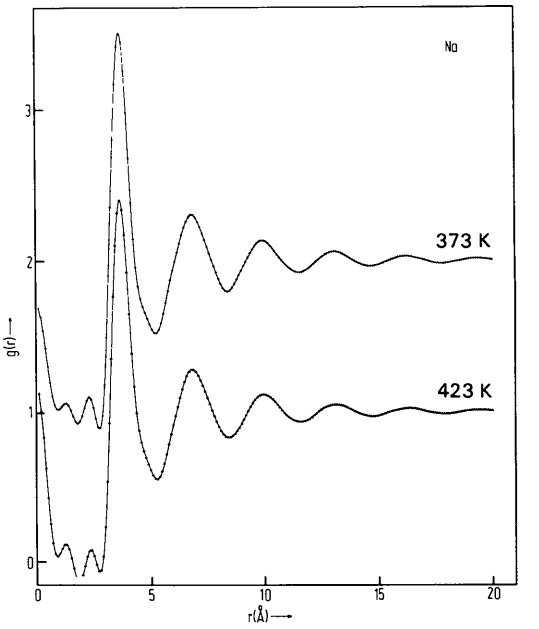

Fig. 16. The radial distribution functions of liquid Na at different temperatures.

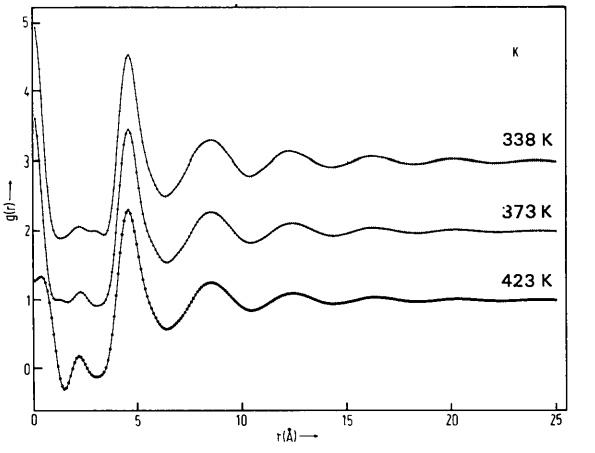

Fig. 17. As Fig. 16, for K.

where r_1 is the point of intersection with the abscissa found by extrapolating the slope of the left-hand side of the first peak. r_2 was chosen in two ways. First, we extrapolated the slope of the right-hand side of the first peak down to the abscissa (giving N_A for the integral). Secondly, we took r_2 at the first minimum in $g(r)$ after the main peak (giving N_B for the integral). N_A, N_B obtained in this way from our experiments are

	N_A	N_B
Na	10·5	13·8
K	10·6	13·4
Cs	10·2	13·2.

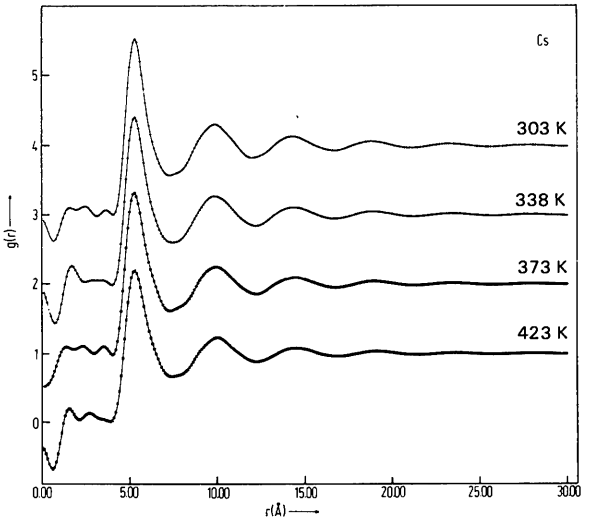

Fig. 18. As Fig. 16, for Cs.

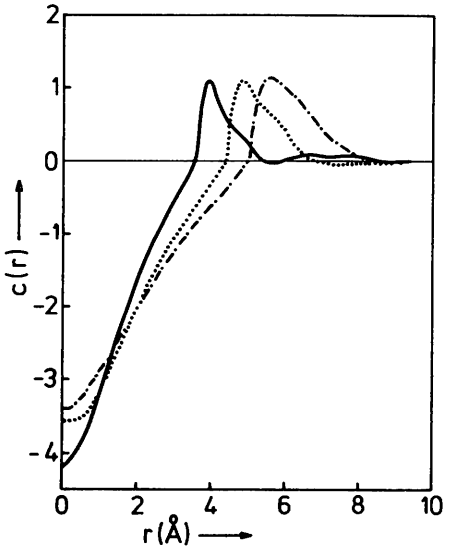

Fig. 19. The direct correlation functions of liquid Na (——), K (····) and Cs (–·–·–) at 373 K. When $c(r)$ passes zero the vertical scale is changed by a factor ten.

The error in N_A and N_b can be estimated to be $\pm 0{\cdot}5$ and originates from the experimental error in $g(r)$ and the error introduced by the extrapolation. We see that the average of N_A and N_B is approximately 12, the number of nearest neighbours in the f.c.c. close-packed structure (which is *not* the common crystal structure of the alkali's: they are usually b.c.c.).

In Fig. 19 we have plotted the direct correlation functions of the three investigated metals, for a temperature of 373 K.

(e) *The pair potential*

In the theory of liquid structure, several approximate relations between the pair distribution function, the direct correlation function and the pair potential $\varphi(r)$ have been proposed. None of these approximations is generally considered to be entirely satisfactory. They are discussed in Hansen & McDonald (1976). We have considered four of them, the mean spherical approximation (MSA), the Born–Green approximation (BG), the Percus–Yevick approximation (PY) and the Hyper-Netted-Chain approximation (HNC). In the MSA, the result is simply

$$\varphi(r) = -k_B\, Tc(r), \tag{4.8}$$

$c(r)$ being given in Fig. 19.

The BG approximation has been investigated by Ailawadi, Banerjee & Choudry (1974), Howells & Enderby (1972), Waseda & Suzuki (1971), Waseda & Ohtani (1973) and Kumaravadivel, Evans & Greenwood (1974). We adopt the conclusion of the last authors that this approximation is unsuitable for deriving the pair potential $\varphi(r)$ from the experimental structure factors. Among other things, it leads to an unacceptable temperature variation of $\varphi(r)$.

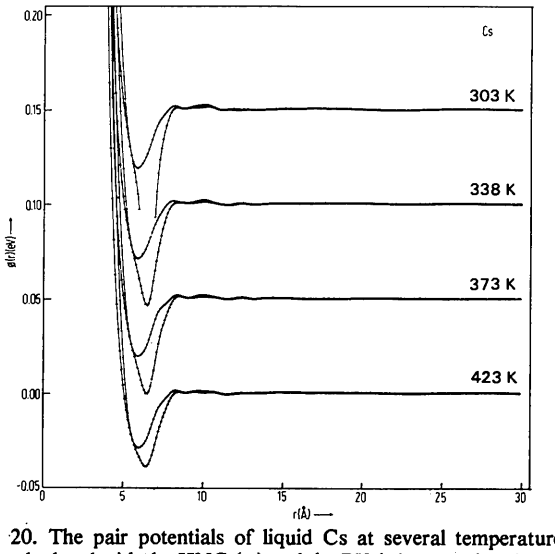

Fig. 20. The pair potentials of liquid Cs at several temperatures calculated with the HNC (+) and the PY (△) approximation.

In the PY and HNC approximations, $\varphi(r)$ is given by

$$\text{(PY)}\ \varphi(r) = k_B T \ln[1 - c(r)/g(r)], \quad (4.9)$$

$$\text{(HNC)}\ \varphi(r) = k_B T[g(r) - c(r) - 1 - \ln g(r)]. \quad (4.10)$$

The two results are compared in Fig. 20 for Cs. In the PY approximation, divergent results are obtained when $c(r)$ and $g(r)$ are of similar magnitude. This may happen near the minimum of the potential. We have dropped such parts from our figures. The instability of the PY solution also manifests itself in an exaggerated temperature dependence. With Howells & Enderby (1972), we conclude that the HNC approximation is best suited for our purpose. In Fig. 21, the pair potential for Cs resulting from this approximation is compared with a theoretical pair-potential based on Heine–Abarenkov–Shaw electron-ion model potentials provided with a Born–Mayer repulsion term [for details, see Lee, Bisschop, van der Lugt & van Gunsteren (1978)]. The agreement is considered to be satisfactory.

(*f*) *Electrical resistivities*

Using Ziman's diffraction model and Heine–Abarenkov–Shaw model potentials (Hallers, Mariën & van der Lugt, 1974) and including screening corrections according to Toigo & Woodruff (1970) we calculated the electrical resistivities ρ of the investigated metals. In Table 3 the calculated and experimental values of ρ and its temperature dependence are listed.

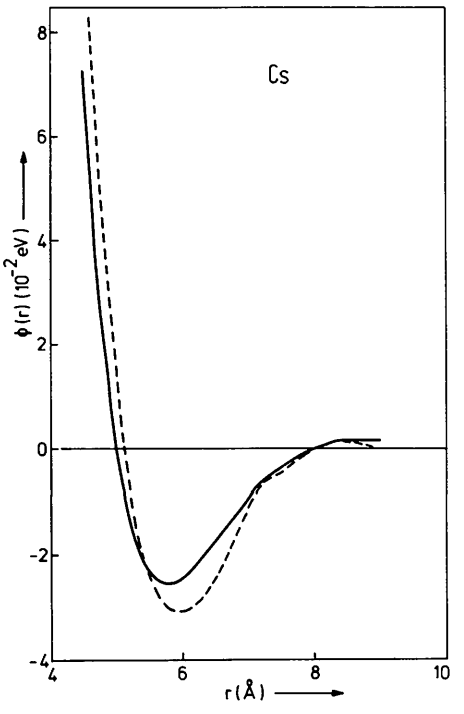

Fig. 21. The pair potential obtained from our X-ray diffraction results for Cs at 373 K in the HNC (– – –) approximation compared with a pair potential derived from a combination of a Heine–Abarenkov-type and Shaw-type model potential (——).

The resistivity formula involves an integral over values of q from zero up to $2k_F$, k_F being the Fermi wavevector of the free-electron gas. As $2k_F$ lies just in front of the first peak of $S(q)$, the resistivity is governed by the small-wavenumber part of the structure factor, which is most sensitive to corrections for multiple scattering. Ignorance of the multiple scattering correction increases the calculated resistivity by a factor up to 10%. For Cs, such (uncorrected) resistivity values were included in a previous publication (Huijben & van der Lugt, 1976).

(*g*) *Comparison of $S(q)$ with theoretical structure factors*

The most commonly used theoretical approximation to the structure factors of liquids is the analytic solution of the Percus–Yevick equation for hard-sphere pair potentials (Ashcroft & Lekner, 1966; Thiele, 1963; Wertheim, 1963). This expression for $S(q)$ involves two parameters: the hard-sphere diameter d and the packing fraction η, which are formally related by

$$\eta = \pi\rho_0 d^3/6. \quad (4.11)$$

The hard-sphere potential is, of course, a poor approximation. Its deficiencies manifest themselves as an exaggerated amplitude and an incorrect phase of the oscillations beyond the main peak of $S(q)$ (Greenfield, Wiser, Leenstra & van der Lugt, 1972). Weeks, Chandler & Anderson (1971) (WCA) and Verlet & Weis (1972) have proposed modifications of the hard-

Table 3. *Calculated resistivities (in* $\mu\Omega$ m $\times 10^2$*) and their temperature derivatives (in* $\mu\Omega$ m/K $\times 10^2$*)*

Experimental resistivity results are added for comparison.

		Calculated		Experimental	
	T (K)	ρ	$\frac{\Delta\rho}{\Delta T}$	ρ	$\frac{d\rho}{dT}$
Na	373	8·32	0·0286	9·6	0·0380
	423	9·75		11·5	
K	338	11·14	0·0494	13·1	0·0543
	373	12·87	0·0524	15·0	0·0520
	423	15·49		17·6	
Cs	303	36·8	0·134	38·3	0·1083
	338	41·5	0·146	42·1	0·1096
	373	46·6	0·104	46·0	0·1112
	423	51·8		51·5	

sphere model. Of these, the Verlet–Weis correction proves to be of minor effect in our case and we will consider only the WCA correction.

WCA introduce a reference system potential which contains only the strong repulsive force, mainly consisting of the Born repulsion and otherwise calculated from a model potential theory (see *e.g.* Lee, Bisschop, van der Lugt & van Gunsteren, 1978). This reference system potential is used in the hard-sphere solution of the Percus–Yevick equation. Additionally, in this equation, an adjusted value of d not obeying (4.11) is used. For the unmodified hard-sphere model as well as for the WCA approximation we have considered two choices for η, obtained by adjusting theoretical and experimental values of $S(q)$ at $q = 0$ and at the first peak, respectively. For Cs, values of η and d are listed in Table 4. Figs. 22 and 23 illustrate the results for $S(q)$ of Cs. The beneficial influence of the WCA correction on the phase and amplitude of the oscillations is evident. For Na and K the results are almost similar. The hump in front of the main peak of the WCA structure factors is an artifact which is typical for this approximation (Ailawadi, Miller & Naghizadeh, 1976). These last authors applied also a modified version of the STLS theory to the calculation of the structure factor of an atomic liquid.

Table 4. *(η,d) parameter couples for the HSPY and WCA structure factors for* Cs *at* 373 K

Structure factor:	HSPY		WCA	
Adjustment	$S(0)$	$S(q_1)$	$S(0)$	$S(q_1)$
η	0·416	0·460	0·416	0·460
d	4·606	4·763	4·999	5·009

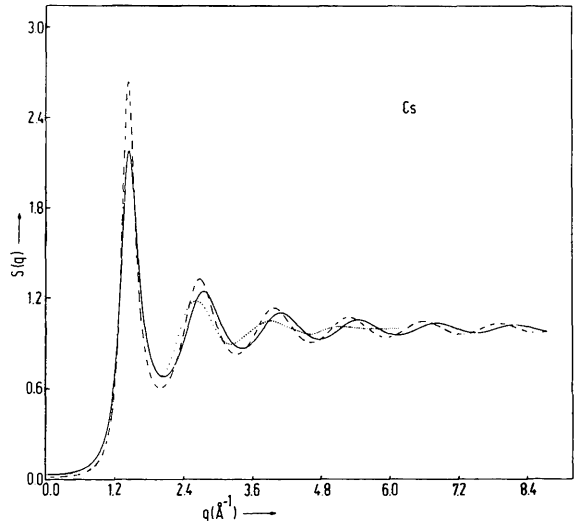

Fig. 22. Structure factor of liquid Cs at 373 K. —— HSPY adjustment of $S(0)$; --- HSPY adjustment of $S(q_1)$; ... experiment.

Generally, the agreement with experiment is comparable with that of the WCA theory. For a comparison the reader is referred to Ailawadi, Miller & Naghizadeh (1976).

Finally, we have carried out computer simulation experiments using pair potentials based on the Heine–Abarenkov–Shaw electron-ion model potentials, of which Fig. 21 gives an illustration. The agreement with experiment is much better than for any of the theoretical approximations dealt with so far in this section. As this computer experiment is described elsewhere, the reader is referred to Lee, Bisschop, van der Lugt & van Gunsteren (1978).

V. Neutron diffraction experiments

Neutron diffraction experiments on liquid Na and Cs were carried out in preparation for an investigation of

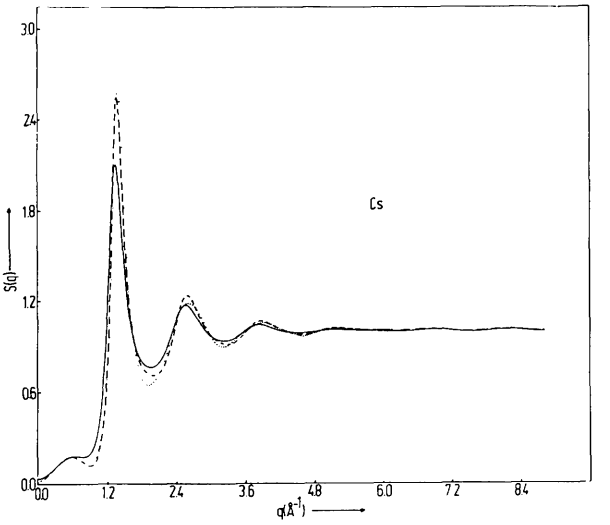

Fig. 23. Structure factor of liquid Cs at 373 K. —— WCA adjustment of $S(0)$; --- WCA adjustment of $S(q_1)$; ... experiment.

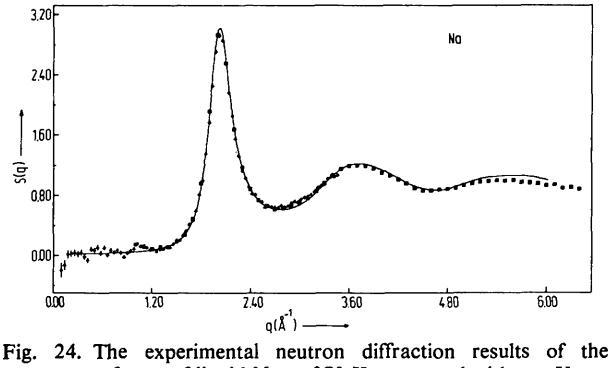

Fig. 24. The experimental neutron diffraction results of the structure factor of liquid Na at 373 K compared with our X-ray diffraction data (——). The measurements with $\lambda = 2{\cdot}58$ Å are represented by △, with $\lambda = 1{\cdot}36$ Å by □.

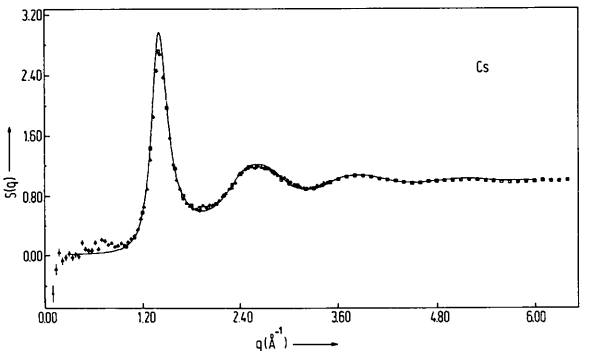

Fig. 25. As Fig. 24, for Cs at 303 K.

liquid Na/Cs alloys. (For alloys, more information is required for a full description of the structure than for a pure metal.)

Fig. 24 shows the results for Na at 373 K. They are compared with our X-ray diffraction data and we see that up to the third oscillation excellent agreement exists, if one takes into account the larger statistical scatter in the neutron data.

For Cs (Fig. 25) agreement with the X-ray data could only be obtained by choosing $\sigma_{inc} = 0{\cdot}095b$ in contrast to the value $\sigma_{inc} = 3{\cdot}20b$ (Shull, 1971). This, of course, is a serious discrepancy which needs further investigation. After this correction, the overall agreement between X-ray and neutron experiments is satisfactory.

The neutron experiments were carried out with the facilities of the Energy Centre Nederland.

The authors thank Dr T. Lee, who carried out the resistivity calculations, Mr J. Roode and Mr J. Numan for their technical assistance and Mr F. van der Horst for many useful discussions. The X-ray equipment was put at our disposal by the crystallographic analysis group of our laboratory. The neutron diffraction measurements were performed in cooperation with Dr C. van Dijk of the ECN, Petten.

This investigation forms part of the research program of the Stichting voor Fundamenteel Onderzoek der Materie (Foundation for Fundamental Research on Matter – FOM), which is financially supported by the Nederlandse Organisatie voor Zuiver Wetenschappelijk Onderzoek (Netherlands Organization for the Advancement of Pure Research – ZWO).

References

AILAWADI, N. K., BANERJEE, P. K. & CHOUDRY, A. (1974). *J. Chem. Phys.* **60**, 2571–2573.

AILAWADI, N. K., MILLER, D. E. & NAGHIZADEH, J. (1976). *Phys. Rev. Lett.* **36**, 1494–1497.

ASCARELLI, P. & GAGLIOTTI, G. (1966). *Nuovo Cimento B*, **43**, 375–388.

ASHCROFT, N. W. & LEKNER, J. (1966). *Phys. Rev.* **145**, 83–90.

CHAN, J. P. (1972). *Phys. Chem. Liq.* **3**, 55–58.

COCKING, S. J. & HEARD, C. R. T. (1965). Harwell Report No. AERE-R5016 (unpublished).

CROMER, D. T. & LIBERMAN, D. (1970). *J. Chem. Phys.* **53**, 1891–1898.

CROMER, D. T. & MANN, J. B. (1967). *J. Chem. Phys.* **47**, 1892–1893.

DOYLE, P. A. & TURNER, P. S. (1968). *Acta Cryst.* A**24**, 390–397.

FABER, T. E. (1972). *Introduction to the Theory of Metals*, p. 113. Cambridge Univ. Press.

GINGRICH, N. S. & HEATON, L. (1961). *J. Chem. Phys.* **34**, 873–878.

GREENFIELD, A. J., WELLENDORF, J. & WISER, N. (1971). *Phys. Rev. A*, **4**, 1607–1616.

GREENFIELD, A. J., WISER, N., LEENSTRA, M. R. & VAN DER LUGT, W. (1972). *Physica (Utrecht)*, **59**, 571–581.

HAJDU, F. & PALINKAS, G. (1972). *J. Appl. Cryst.* **5**, 395–401.

HALLERS, J. J., MARIËN, T. & VAN DER LUGT, W. (1974). *Physica (Utrecht)*, **78**, 259–272.

HANSEN, J. P. & MCDONALD, I. R. (1976). *Theory of Simple Liquids*. London: Academic Press.

HARRISON, W. A. (1966). *Pseudopotentials in the Theory of Metals*, p. 134. New York: Benjamin.

HOWELLS, W. S. & ENDERBY, J. E. (1972). *J. Phys. C*, **5**, 1277–1283.

HUIJBEN, M. J., VAN HASSELT, J. PH., VAN DER WEG, K. & VAN DER LUGT, W. (1976). *Scr. Metall.* **10**, 571–574.

HUIJBEN, M. J., KLAUCKE, H., HENNEPHOF, J. & VAN DER LUGT, W. (1975). *Scr. Metall.* **9**, 653–656.

HUIJBEN, M. J. & VAN DER LUGT, W. (1976). *J. Phys. F*, **6**, L225–229.

International Tables for X-ray Crystallography (1962). Vol. III. Birmingham: Kynoch Press.

KERR, K. A. & ASHMORE, J. P. (1974). *Acta Cryst.* A**30**, 176–179.

KIM, M. G., KEMP, K. A. & LETCHER, S. V. (1971). *J. Acoust. Soc. Am.* **49**, 706–712.

KOLLMANSBERGER, G., FRITSCH, G. & LÜSCHER, E. (1970). *Z. Phys.* **233**, 308–323.

KUMARAVADIVEL, R., EVANS, R. & GREENWOOD, D. A. (1974). *J. Phys. F*, **4**, 1839–1848.

LEE, T., BISSCHOP, J., VAN DER LUGT, W. & VAN GUNSTEREN, W. F. (1978). *Physica (Utrecht)*, **93***B*, 59–62.

MALET, G., CABOS, C., ESCANDE, A. & DELORD, P. (1973). *J. Appl. Cryst.* **6**, 139–144.

MARSHALL, W. & LOVESEY, S. W. (1971). *Theory of Thermal Neutron Scattering*. Oxford: Clarendon Press.

NOVIKOV, I. I., TRELIN, YU. S. & TSYGANOVA, T. A. (1970). *Teplofiz. Vys. Temp.* **8**, 450–451.

NUNES, A. C. & SHIRANE, G. (1971). *Nucl. Instrum. Meth.* **95**, 445–452.

OEHME, H. & RICHTER, H. (1966). *Naturwissenschaften*, **53**, 16.

PAALMAN, H. H. & PINGS, C. J. (1963). *Rev. Mod. Phys.* **35**, 389–399.

PLACZEK, G. (1952). *Phys. Rev.* **86**, 377–388.

POWLES, J. G. (1973*a*). *Mol. Phys.* **26**, 1325–1350.

POWLES, J. G. (1973*b*). *Adv. Phys.* **22**, 1–56.

RAHMAN, A., SINGWI, K. S. & SJÖLANDER, A. (1962*a*). *Phys. Rev.* **126**, 986–996.
RAHMAN, A., SINGWI, K. S. & SJÖLANDER, A. (1962*b*). *Phys. Rev.* **126**, 997–1004.
RISTE, T. (1970). *Nucl. Instrum. Meth.* **86**, 1–4.
SCHIERBROCK, R. B., LANGNER, G., FRITSCH, G. & LÜSCHER, E. (1972). *Z. Naturforsch. Teil A*, **27**, 826–832.
SHULL, C. G. (1971). *Neutron Cross Section Data*, compilation 1971. M.I.T.
SMELSER, S. C., HENNINGER, E. H., PINGS, C. J. & WIGNALL, G. D. (1975). *J. Appl. Cryst.* **8**, 8–11.
THIELE, E. (1963). *J. Chem. Phys.* **39**, 474–479.
TOIGO, F. & WOODRUFF, T. O. (1970). *Phys. Rev. B*, **2**, 3958–3966.
VERLET, L. & WEIS, J. J. (1972). *Phys. Rev. A*, **5**, 939–952.
VINEYARD, G. H. (1954). *Phys. Rev.* **96**, 93–98.
WAGNER, C. N. J. (1972). *Liquid Metals*, edited by S. Z. BEER, pp. 257–329. New York: Marcel Dekker.
WAGNER, C. N. J. (1977). *Liquid Metals* 1976, edited by R. EVANS & D. A. GREENWOOD, Conference Series Number 30, pp. 110–116. Bristol and London: The Institute of Physics.
WASEDA, Y. & OHTANI, M. (1973). *Sci. Rep. Res. Inst. Tohoku Univ. Ser. A*, **24**, 218–240.
WASEDA, Y. & SUZUKI, K. (1971). *Phys. Status Solidi B*, **47**, 203–210.
WASEDA, Y. & SUZUKI, K. (1973). *Sci. Rep. Res. Inst. Tohoku Univ. Ser. A*, **24**, 139–184.
WEEKS, J. D., CHANDLER, D. & ANDERSEN, H. C. (1971). *J. Chem. Phys.* **54**, 5237–5247.
WERTHEIM, M. S. (1963). *Phys. Rev. Lett.* **10**, 321–323.
WOLFF, P. M. DE (1948). *Appl. Sci. Res. Sect. B*, **1**, 119–126.
YARNELL, J. L., KATZ, M. J., WENZEL, R. G. & KOENIG, S. H. (1973). *Phys. Rev. A*, **7**, 2130–2144.
ZIMAN, J. M. (1961). *Philos. Mag.* **6**, 89–138.

Acta Cryst. (1979). A**35**, 445–448

Dynamic Deformation Effects on the Debye–Waller Factor

BY JOHN S. REID

Department of Natural Philosophy, The University, Aberdeen, AB9 2UE, Scotland

(*Received* 13 *November* 1978; *accepted* 19 *December* 1978)

Abstract

The effect on the Debye–Waller factors of having scattering factors which depend on atomic motion is developed through the reciprocal-space formulation. The resulting dependence of the Debye–Waller B on the scattering vector is of a simple form when a shell model adequately represents the deformation of the electron distribution. Numerical results are presented, without any serious approximations, for the governing constant appropriate to six alkali halides and explicit results are given for $\Delta B_k/B_k$ for NaF, NaCl and KCl. A comparison with the recent real-space formulation of March & Wilkins [*Acta Cryst.* (1978), A**34**, 19–26] suggests that the reciprocal-space approach might be more fruitful.

Introduction

Dynamic deformation refers to the change in the scattering factor of an atom caused by the thermal motion both of the atom itself and of all other atoms in the crystal. The effect on the kth type of atom in the lth unit cell depends on the scattering vector **K**. Appropriate coupling parameters $\beta(l'-l, kk', \mathbf{K})$ were introduced in slightly reduced generality by Born (1942) and have been discussed in particular by Reid (1974) and March & Wilkins (1978). The latter concentrated on real-space parameters to determine entirely in terms of real-space quantities the resulting changes in the Debye–Waller factors. They showed how the changes were given by an expression which involved all the $\beta(l'-l, kk', \mathbf{K})$ for a lattice but the inevitable lack of knowledge of these parameters forced drastic simplifications before a usable expression could be obtained. Consequently, although they quoted results relevant to typical shell-model distortions (for NaCl and NaF), there is still considerable uncertainty as to the magnitude of the dynamic deformation effect on the Debye–Waller factor shown by current lattice-dynamical models.

The present paper concentrates on the reciprocal-space formulation for the effect of ionic deformation and shows that a simple form is obtained for the modification of the Debye–Waller factor by shell-model distortions. The result is that the effective Debye–Waller factor depends on the scattering vector **K** by an amount which can be calculated with a shell model. The size and variation of this effect is illustrated for some alkali halides and a brief comparison made with the results of March & Wilkins (1978).

0567-7394/79/030445-04$01.00